Heterojunctions between metals and carbon nanotubes as ultimate nanocontacts

Julio A. Rodríguez-Manzo[a], Florian Banhart[a,1], Mauricio Terrones[b], Humberto Terrones[b], Nicole Grobert[c], Pulickel M. Ajayan[d], Bobby G. Sumpter[e], Vincent Meunier[e], Mingsheng Wang[f], Yoshio Bando[f], and Dmitri Golberg[f]

[a]Institut de Physique et Chimie des Matériaux, Unité Mixte de Recherche 7504, Université de Strasbourg, 23 Rue du Loess, 67034 Strasbourg, France; [b]Laboratory for Nanoscience and Nanotechnology Research and Advanced Materials Department, Instituto Potosino de Investigación Científica y Tecnológica, Camino a la Presa San José 2055, Col. Lomas 4a Sección, 78216 San Luis Potosí, México; [c]Department of Materials, University of Oxford, Parks Road, Oxford OX1 3PH, United Kingdom; [d]Department of Mechanical Engineering and Materials Science, Rice University, P.O. Box 1892, Houston, TX 77251-1892; [e]Computer Science and Mathematics Division and Center for Nanophase Materials Sciences, Oak Ridge National Laboratory, P.O. Box 2008, Oak Ridge, TN 37831-6367; and [f]World Premier International Center for Materials Nanoarchitectonics, National Institute for Materials Science, Namiki 1-1, Tsukuba, Ibaraki 305-0044, Japan

Communicated by Mildred S. Dresselhaus, Massachusetts Institute of Technology, Cambridge, MA, January 29, 2009 (received for review December 29, 2008)

We report the controlled formation and characterization of heterojunctions between carbon nanotubes and different metal nanocrystals (Fe, Co, Ni, and FeCo). The heterojunctions are formed from metal-filled multiwall carbon nanotubes (MWNTs) via intense electron beam irradiation at temperatures in the range of 450–700 °C and observed in situ in a transmission electron microscope. Under irradiation, the segregation of metal and carbon atoms occurs, leading to the formation of heterojunctions between metal and graphite. Metallic conductivity of the metal–nanotube junctions was found by using in situ transport measurements in an electron microscope. Density functional calculations show that these structures are mechanically strong, the bonding at the interface is covalent, and the electronic states at and around the Fermi level are delocalized across the entire system. These properties are essential for the application of such heterojunctions as contacts in electronic devices and vital for the fabrication of robust nanotube–metal composite materials.

nanoelectronics | interfacial interactions | conductivity | electron microscopy | composites

Heterojunctions between different materials are of increasing interest in nanotechnology. For creating devices at the nanoscale, different structures have to be joined so as to obtain junctions with predefined properties. Junctions between carbon nanotubes (CNTs) and metals (1–3) or semiconducting (1, 4) nanowires are highly desirable to exploit the excellent electronic and mechanical properties of CNTs. In electronic devices, conductive contacts between the graphitic network of CNTs and metallic electrodes need to be established to link the nanotubes with each other and their periphery. To date, most results indicate that the properties of such a device are dominated by the electronic behavior at the nanotube–metal contact. For instance, the resistance of the ohmic contact (1, 3, 5) or Schottky barrier effects (6) are influenced by the type of interface between metal and the graphitic structure. In some previous studies, multiwall carbon nanotube (MWNTs) interconnections with metal electrodes only occurred with the outermost wall of MWNTs (7). A robust mechanical connection in such a junction cannot be expected, nor can the inner walls of MWNTs participate considerably in charge transport (5). Therefore, detailed knowledge regarding the nature and strength of bonding as well as the morphology and electrical properties of contacts is important because it is vital to connect all concentric cylinders of a MWNT, across the entire cross-section of the nanotube, to a metal particle. In particular, a covalent nanotube–metal junction would allow one to attach nanotubes firmly to metal pieces, which is useful for achieving well-defined electrical contacts and also for attaching nanotubes firmly to metal supports for the realization of ultrastrong nanotube ropes in mechanical systems.

Recent studies have reported examples of graphitic material interfaces with metal particles for Co crystals and nanotubes (8), Fe particles with amorphous carbon pillars (9), and W (10) or Pt (3) particles and MWNTs. An interface between carbon nanotubes and metal particles was also observed during the growth of nanotubes from catalytically active metals (11). However, the structure of the interface and the nature of bonding between metal and carbon remained unclear. This is not only important for predicting and understanding the electrical or mechanical properties of the junctions but also for exploring the growth of nanotubes from catalytically active metal particles where the nucleation and growth of the tube occur through such an interface

Here, we report a technique for the efficient formation of nanotube–metal heterojunctions in which the metal is strongly bonded to all layers of a MWNT. The controlled process is carried out and observed in a transmission electron microscope (TEM). It involves intense electron irradiation of metal-filled MWNTs at temperatures of 450–700 °C whereby real-time in situ imaging with lattice resolution is possible (12–14). It has recently been demonstrated that materials can be tailored at the nanoscale by controlled electron irradiation, e.g., metal nanostructures (14) and CNTs (15). In particular, metal-filled CNTs have shown interesting phenomena when exposed to an intense electron beam (16, 17). In the present study, rod-like structures are obtained, consisting of 2 MWNT segments joined by short transition metal nanowires, also termed in this study as MWNT–*m*–MWNT junctions, where *m* stands for a metal or a metallic alloy. We complement the experimental evidence by performing density functional theory (DFT) calculations to elucidate the atomistic details of the carbon–metal interface. We also provide experimental and theoretical evidence that the so-formed metal–MWNT contacts exhibit a high transmission amplitude for electron transport across the interface.

Results

Specimens of Fe-, Co-, Ni- and FeCo-filled MWNTs were synthesized (18, 19) as described in the materials and methods section below. Electron irradiation experiments were carried out in an electron microscope by focusing an electron beam with a diameter in the range 2–20 nm, resulting in current densities of $10^3 - 10^5$ A/cm^2, onto metal-filled nanotubes. Thus, carbon

Author contributions: F.B., M.T., H.T., and P.M.A. designed research; J.A.R.-M., M.T., P.M.A., B.G.S., V.M., M.W., and D.G. performed research; N.G. contributed new reagents/analytic tools; F.B., B.G.S., V.M., M.W., Y.B., and D.G. analyzed data; and J.A.R.-M., F.B., M.T., H.T., N.G., P.M.A., B.G.S., V.M., M.W., Y.B., and D.G. wrote the paper.

The authors declare no conflict of interest.

[1]To whom correspondence should be addressed. E-mail: banhart@ipcms.u-strasbg.fr.

This article contains supporting information online at www.pnas.org/cgi/content/full/0900960106/DCSupplemental.

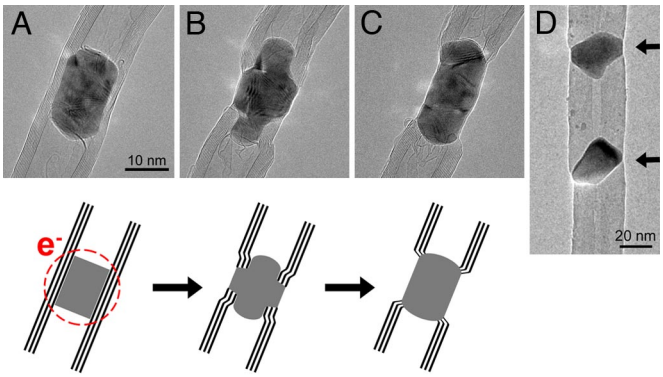

Fig. 1. Formation of a MWNT–Co–MWNT junction from a Co-filled MWNT subjected to electron irradiation (200 keV) at 700 °C. (*A*) The Co-filled MWNT at the beginning of the experiment. (*B*) The focused electron beam damages the tube, and the Co nanowire is expelled to the surface, experiencing shape changes after 6 min of irradiation. (*C*) Finally, the Co particle acts as a link between the 2 MWNT segments. The time required to obtain the final shape was 11 min. The sketch at the bottom shows the mechanism of the process. The circle indicates the zone subjected to electron irradiation. (*D*) Periodic FeCo–MWNT heterojunction, formed by repeated irradiation at different positions of a FeCo-filled nanotube. Arrows indicate metal particles.

atoms from the MWNT walls were displaced ballistically by the energetic electrons. An elevated specimen temperature of 450–700 °C was chosen to allow annealing of beam-induced damage in the graphitic lattice, thereby avoiding the agglomeration of structural defects (12, 20). At the electron energies in our experiments, atom displacements occur only in the MWNTs but not in the encapsulated metals, which have much higher atom displacement thresholds than graphitic carbon (12). Nevertheless, shape changes of the metals occur by the compressive action of the graphitic layers (17) and, once the metal surface is not covered anymore by graphite, because of surface migration of atoms under the electron beam.

Fig. 1 shows the process by which a MWNT–metal junction is formed. The electron beam was converged onto a small region of a Co-filled tube (2–5 nm in diameter), causing the displacement of carbon atoms from the tube walls. Consequently a reconstruction of the encapsulated Co nanowire is driven by shape changes of the nanotube and interdiffusion between the 2 components. The graphitic layers within the MWNT (Fig. 1*A*) reconstruct, causing the Co crystal to change its shape and segregate (Fig. 1*B*). The reshaping of the Co nanowire continues, and a MWNT–Co–MWNT junction is finally obtained (Fig. 1*C*). The complete process took 11 min at an irradiation intensity of $\approx 10^4$ A/cm^2. Another example is shown in supporting information (SI) Fig. S1. This process can be controlled and extended to produce periodic arrays by repeated irradiation, as shown in Fig. 1*D*, where a FeCo-filled MWNT was transformed into a structure where 3 MWNT segments are connected by 2 metal particles.

High-resolution scanning transmission (STEM) and TEM electron microscopy images depicting the detailed atomic structure of metal–MWNT interfaces are shown in Fig. 2. For Co (Fig. 2*A*) the STEM lattice image (obtained with an aberration-corrected probe) of the Co crystal shows the [110] zone axis projection of the Co fcc lattice. Although the MWNT axis appears to be aligned parallel to the [−110] axis of the Co particle, the graphitic basal layers are bent toward (111) Co planes at the intersection. This was observed in many examples where (111) planes of the metal crystals were visible. Because the metal crystals do not have the rotational symmetry of the tube, the bonding between (111) planes of the metal and the layers of the tube can only occur locally along the circumference of the

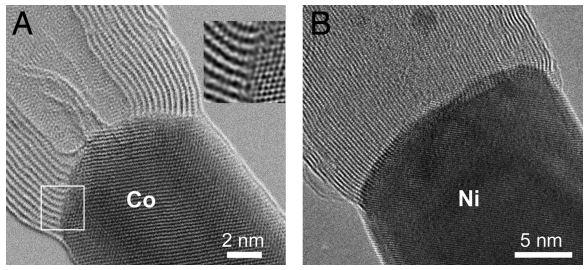

Fig. 2. High-resolution images from metal–MWNT junctions. (*A*) Bright-field STEM image (C_s-corrected) of a MWNT–Co interface. The Co particle has an fcc structure (the image shows an alignment close to the [110] zone axis projection of the Co fcc lattice). Strain is introduced at the interface as can be seen by the local bending of the graphitic layers at the interface. The *Inset* shows a detail of the interface (white square) after noise filtering, where the bending of the nanotube layers to match the metal lattice is visible. (*B*) HRTEM image of a MWNT–Ni interface. The Ni particle has an fcc structure.

tube, but this type of bonding seems to be favorable. A semicoherent interface appears to compensate the large lattice mismatch between the metal and the nanotube lattice (Fig. 2*A Inset*). Given the fact that the mismatch is extreme and the interface must be quite disordered locally, the strain at the interface (seen as the bending of the MWNT walls) is considerable and shows that the bonding between the nanotube and Co must be strong. Fig. 2*B* shows a TEM image of the interface for Ni, where a thicker Ni-filled MWNT was used as a starting material. It is possible to observe the mismatch between the MWNT and the Ni crystal as well as dark contrast close to the interface, again indicating strong bonding. No indications for the formation of carbides, even in lowest quantities close to the interface, were found by imaging and electron nanodiffraction. The metal crystals always appeared in the fcc phase. Electron energy-loss spectroscopy (EELS) did not show particular features at the interface (see Fig. S2).

To evaluate the electrical transport through a MWNT–*m*–MWNT system, direct transport measurements were carried out in another electron microscope equipped with a dedicated STM-TEM holder (21) (Fig. 3). A single Co-filled MWNT

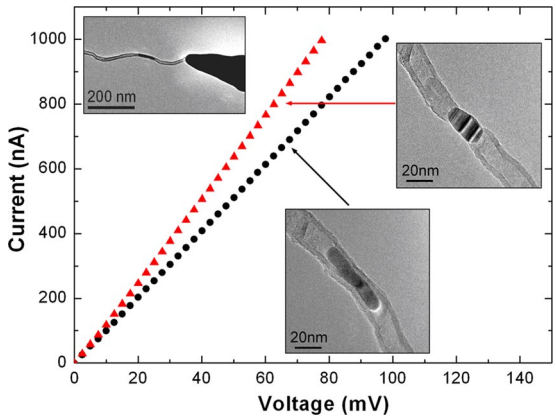

Fig. 3. Representative I–V curves taken from a Co-filled MWNT (black dots) and from the same tube subjected to e-beam irradiation and with a MWNT–Co–MWNT joint (red triangles) measured by using the STM-TEM "Nanofactory" setup. The current range was limited <1 μA to avoid overheating of the structure. The *Insets* display the corresponding TEM images. (*Upper Left*) A Co-filled MWNT attached to a gold wire (biased far to the left) connected to the Au STM tip inside the electron microscope. ((*Lower Center*) the appearance of the starting nanotube in the "filled" state. (*Upper Right*) The same tube after biasing (to induce Joule heating) and irradiation resulted in the Co-joint formation.

protruding from the edge of a gold wire (biased) was connected to a gold tip (*Left Inset* in Fig. 3). A bias applied to the structure was slowly increased until a Co particle began to melt (because of Joule heating) and move. The bias was then immediately reduced to prevent further shrinking or moving of the particle. At this moment, we found that the conduction was indeed improved, which is mainly attributed to the achievement of a better electrical contact (22). The I–V curves became smooth, which indicates a good and stable electrical contact has been established because of structure annealing under biasing. The electron beam was then converged onto the particle. During the irradiation, a bias of a few volts was applied to keep the tube at a high temperature and to prevent structural failure under irradiation. During this process, the current through the tube was $\approx$25 μA. Then, and in line with the above-mentioned facts, a MWNT–Co–MWNT junction was finally formed (*Upper Right Inset* in Fig. 3), and I–V curves were recorded.

The Co particle-joined structure clearly shows metallic conduction without any semiconducting behavior or band offsets. The nature of the junction (simultaneous conduction in both directions: MWNT–Co–MWNT) allows us to exclude diode effects. Four analogous experiments were performed on various tubes by paying special attention to a comparison of the resistances of filled vs. Co-joined structures (Fig. S3). In all cases, the transport behavior was similar—the resistance of the "joined" state was always slightly lower than the original "filled" state. For example, the resistance of the curves shown in Fig. 3 was measured to be 98 kΩ (filled state, black plot) and 78 kΩ (Co-joined state, red plot). The rather high initial resistance in these cases might be due to defects in the nanotubes, but it is shown that the formation of junctions improves the situation.

To develop a fundamental understanding of the nature of the nanotube–metal system, we performed first-principles electronic structure calculations based on DFT, by using a SWNT–Co heterojunction as a model. The electronic structure of the SWNT–Co system was examined by using the Vienna ab initio simulation package (VASP), version 4.6.6 (23–26). The Kohn–Sham equations were solved by using the projector augmented wave (PAW) approach (27, 28) and a plane-wave basis with a 400-eV energy cutoff. The single heterojunction interface was modeled with a (9, 0) SWNT and a Co cluster. The cell size was $20 \times 20 \times 32$ Å^3 providing a vacuum layer of at least 12 Å on either side whereby one end of the nanotube was passivated with H. The model included a total of 192 atoms (75 are Co; 3 layers of 5×5). A superstructure calculation was also performed by periodically repeating the heterojunctions. In that case, the electronic properties of the resulting $20 \times 20 \times 22$-Å^3 unit cell was treated with a $1 \times 1 \times 4$ Brillouin zone Monkhorst–Pack sampling. The generalized gradient approximation (GGA) exchange-correlation functional of Perdew, Burke, and Ernzerhof (29) was used for all of the calculations. Electronic convergence was defined as a consistency between successive cycles of $<10^{-3}$ eV, and all calculations were performed by assuming spin-polarized electrons. From the fully optimized SWNT–Co periodic heterojunction we computed both the planar and macroscopic average (30, 31) of the local potential and found that a smooth transition between the 2 materials is formed at the interface. Relaxation at the interface is important to avoid interface states stemming from the existence of unsaturated dangling bonds from carbon.

The fully optimized (theoretical) superstructure made up of a Co cluster interacting with a (9, 0) SWNT is shown in Fig. 4*A* (one unit cell is shown). We used the finite size calculation with hydrogen-passivated carbon ends to compute the binding energy between the 2 components of the heterostructure via [E(SWNT–Co) − E(SWNT)–E(Co)]. This gives a surprisingly large value of 68.46 eV. Assuming there are 9 bonds formed (from the 9 dangling C bonds of the nanotube) the corresponding bond energy is 7.6 eV per bond. From previous studies of single benzyl radicals interacting with transition metals (32), we found that a moderately strong chemical bond is formed to the metals with binding energies larger for those having less filled *d* orbitals (left side of the periodic table). The binding energy for a Co slab and a single benzyl radical (benzyl is sanding up from the surface) is on the order of 2 eV, considerably smaller than that determined for the Co–SWNT–Co heterostructure of the present study. Examination of the interatomic distances of the structure in Fig. 4*A* reveals that there are multiple C–Co interactions (as many as 3 per carbon), each of which can contribute significantly to the total binding energy. The nature of the bonding is elucidated in charge density isocontours of Fig. 4 *B–D*. In particular, metallic binding is apparent in the Co section, whereas covalent (directional) binding is clearly present in the nanotube section and at the interface between the tube and the metallic particle. The electronic structure near the Fermi level is shown in Fig. 4*E*. The charge density isosurface corresponding to the highest valence state of the heterojunction formed from the Co cluster and (9, 0) SWNT is shown (in blue) along with the conduction state (red). There is considerable delocalization across the entire system, which confirms the metallic nature of the heterostructure. The strong binding and the delocalization between Co and the nanotube indicate that the electronic transport across the interfaces will not be predominantly determined by tunneling (as it would be for weak binding such as van der Waals bonds) and can therefore accommodate large current flow (33).

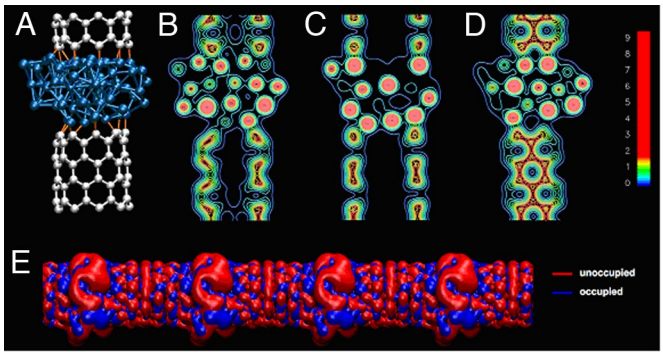

Fig. 4. Summary of DFT results. (*A*) DFT-optimized structure for a (9, 0) single-walled carbon nanotube/Co periodic heterojunction (see Fig. 1). The bonds between the Co atoms and the carbon atoms are highlighted in orange and have been drawn by using a cutoff of 2.1 Å. (*B–D*) Isocontour plots of the charge density for 3 different longitudinal planes cut parallel to the system's axis. Metallic binding is apparent in the Co section, whereas covalent (directional) binding can be seen both in the nanotube section and at the interface between the tube and the metallic particle. The atomic positions in the ball-and-stick representation are drawn in correspondence to the 3 isocontour plots. The units of the color bar are in electrons/Å^3. (*E*) Isosurface plots ($q = 10^{-6}$ electrons per Å^3) of the charge density in a periodic multijunction system at the Fermi level (red, density integrated in a small window of 0.2 eV below the Fermi level; blue, in a 0.2 eV window above the Fermi level).

Discussion

The morphology of carbon nanotubes filled with thin metal wires is unfavorable from an energetic viewpoint. Materials with surface energies $>$0.1 J/m^2 do not wet graphitic surfaces (34). The surface energy for crystalline Fe or Co is $\approx$2.5 J/m^2 (35). Consequently, the metal tends to reduce its surface area to minimize energy. Minimization of surface or interface energies would favor a metal crystal with the smallest possible surface-to-volume ratio that is not a wire but a spherical particle. However, the high morphological stability of nanotubes normally hinders such a transformation into an elongated interface energy-optimized structure. When a metal nanowire encapsulated in a nanotube is exposed to an electron

beam that displaces carbon atoms, a morphological transformation of the graphitic shell can take place. Because the metal particles remain crystalline during the transformation, surface minimization of the metal occurs by self-diffusion. Electron irradiation causes atom displacements and leads to an intermixing of the 2 phases (carbon atoms diffuse into the metal and metal atoms diffuse through the graphitic shells). A certain mobility of carbon in the metal crystal and of metal atoms in the graphitic shells allow the segregation of the 2 phases. It is remarkable that the shape of the nanotubes is recovered after the reconstruction, whereas the metal crystal develops a low-aspect-ratio geometry.

According to our observations, 2 mechanisms seem to drive the process from which a metal-filled MWNT is transformed into a MWNT–*m*–MWNT junction:

First, the diffusion of carbon atoms into and through the metal crystal is of major importance in the growth of carbon nanotubes from catalytically active metal crystals (16). Although the solubility of carbon in transition metals such as Co or Fe is low, the high diffusivity permits an efficient transport of carbon through the metal (36). Because carbon atoms are easily displaced from the shells at an electron energy of 200 keV, we may assume that a certain amount of carbon is implanted into the metal crystal where carbon diffusion is fast and allows an efficient transfer of the atoms to the end of the metal particles.

Second, metal atoms diffuse through the shells of the nanotube. It has been shown in earlier studies of metal–carbon nanocomposites that the exposure of metal crystals encapsulated in graphite shells to electron irradiation leads to the migration of metal atoms through the graphitic shells (37, 38). This process is driven by the compression of graphitic cages under electron irradiation, forcing the metal atoms to occupy vacancies in the graphitic lattice and to migrate toward the region of low pressure, i.e., to the surface of the particles, which also appears to happen in the present experiment, as seen in Figs. 1 and 2.

Nanotubes under an electron beam contract and develop high pressure onto the encapsulated materials (17), leading to an extrusion of the metal crystal or, when the tube has already collapsed in the previously empty regions, to the gradual displacement of the metal through the shells. The segregation of carbon and metal leads to the junction where strong bonds between the 2 phases develop, as seen in Fig. 2. We can assume that only strong covalent bonds are able to lead to such a highly strained interface, and the electrical measurements as well as the electronic structure calculations indeed indicate the presence of covalent bonds. The formation of metal–carbon bonds at the junction can contribute again to the minimization of interface energy. As mentioned above, we have quantified the covalent nature of the nanotube–Co–nanotube heterojunction by directly computing the binding energy and by examining the charge density at the interface (Fig. 4 *B–D*). The electronic structure shown in Fig. 4*E* has significant delocalization across the entire heterostructure, indicating a metallic character, which was indeed confirmed by the direct transport measurements.

In conclusion, we have demonstrated that it is possible to generate MWNT–*m*–MWNT junctions with promising transport properties via electron irradiation of metal–nanotube composite structures. The computed electronic structure for the model nanotube–Co heterojunction shows that these types of structures have a potential for engineering functional electronic and ferromagnetic devices. The magnetotransport properties and possible applications in memory devices are certainly worth exploring. An upscaling of the technique by applying focused ion beams could be feasible. The structures and the technique to create them should set the stage for future fabrication of contacts in devices that are mechanically and electrically robust. Three dimensional metal-nanotube networks could be foreseen as extremely robust nanocomposites.

Materials and Methods

Metal-filled MWNTs were synthesized by aerosol pyrolysis (18, 19). For producing Fe-, Co-, Ni- and FeCo-filled MWNTs, solutions (3 wt % solute-to-solvent) of ferrocene, Co acetylacetonate II, nickelocene, or a mixture of ferrocene and cobaltocene dissolved in toluene or ethanol were used, respectively. The solutions were mixed with Ar so as to produce an aerosol that was directed into a quartz tube placed inside a furnace at 850 °C. After the reaction, MWNTs partly filled with metal nanowires were scraped from the quartz tube walls and dispersed in ethanol by sonication. Finally, a drop of the suspension was deposited onto a TEM grid. The samples were heated to 450–700 °C by using a heating stage in the TEM. Electron irradiation experiments and imaging were carried out by using a field emission TEM/STEM (JEOL 2100F, operated at 200 kV) with a C_s-corrected illumination system. Irradiation experiments and imaging were carried out in the TEM mode of the instrument. Some high-resolution images were taken in the STEM mode (where the spot is too localized for irradiating the whole diameter of the nanotubes). Transport measurements were carried out in a JEM-3100FEF field-emission TEM (Omega Filter) using a Nanofactory Instruments piezo-driven STM-TEM holder (21).

ACKNOWLEDGMENTS. We thank I. Janowska for assistance in the preparation of some nanotube samples. This work was supported by Deutsche Forschungsgemeinschaft Grant Ba 1884/6-1; CONACYT-Mexico Grants 56787 (Laboratory for Nanoscience and Nanotechnology Research), 45762 (to H.T.), 45772 (to M.T.), 58899 Inter American Collaboration (to M.T.), Fondo Mixto de San Luis Potosí 63001 S-3908 (to M.T.), 2004-01-013/SALUD-CONACYT (to M.T.), and Fondo Mixto de San Luis Potosí 63072 S-3909 (to H.T.); the Royal Society (N.G.); National Science Foundation support for the Materials World Network Program under Grant DMR-0801012 (to P.M.A.); the Center for Nanophase Materials Sciences, sponsored by the Division of Scientific User Facilities, U.S. Department of Energy, and by the Division of Materials Science and Engineering (B.G.S. and V.M.); and the World Premier International Center (MANA) of the National Institute for Materials Science, Tsukuba, Japan (M.S.W., Y.B., and D.G.)

1. Zhang Y, Ichihashi T, Landree E, Nihey F, Iijima S (1999) Heterostructures of single-walled carbon nanotubes and carbide nanorods. *Science* 285:1719–1722.
2. Luo J, Zhang L, Zhang Y, Zhu J (2002) Controlled growth of one-dimensional metal-semiconductor and metal-carbon nanotube heterojunctions. *Adv Mater* 14:1413–1414.
3. Asaka K, Nakahara H, Saito Y (2008) Nanowelding of a multiwalled carbon nanotube to metal surface and its electron field emission properties. *Appl Phys Lett* 92:023114.
4. Hu J, Ouyang M, Yang P, Lieber C (1999) Controlled growth and electrical properties of heterojunctions of carbon nanotubes and silicon nanowires. *Nature* 399:48–51.
5. Li H, Lu W, Li J, Bai X, Gu C (2005) Multichannel ballistic transport in mutiwall carbon nanotubes. *Phys Rev Lett* 95:086601.
6. Tans S, Verschueren A, Dekker C (1998) Room-temperature transistor based on a single carbon nanotube. *Nature* 393:49–52.
7. Collins PG, Arnold MS, Avouris P (2001) Engineering carbon nanotubes and nanotube circuits using electrical breakdown. *Science* 292:706–709.
8. Jensen K, Mickelson W, Han W, Zettl (2005) A Current-controlled nanotube growth and zone refinement. *Appl Phys Lett* 86:173107.
9. Ichihashi T, Fujita J, Ishida M, Ochiai Y (2004) In situ observation of carbon-nanopillar tubulization caused by liquidlike iron particles. *Phys Rev Lett* 92:215702.
10. Jin C, Suenaga K, Iijima S (2008) Plumbing carbon nanotubes. *Nat Nanotechnol* 3:17–21.
11. Yoshida H, Takeda S, Uchiyama T, Kohno H, Homma Y (2008) Atomic-scale in-situ observation of carbon nanotube growth from solid state iron carbide nanoparticles. *Nano Lett* 8:2082–2086.
12. Banhart F (1999) Irradiation effects in carbon nanostructures. *Rep Prog Phys* 62:1181–1221.
13. Krasheninnikov AV, Banhart F (2007) Engineering of nanostructured carbon materials with electron or ion beams. *Nat Mater* 6:723–733.
14. Fischbein MD, Drndić M (2007) Sub-10 nm device fabrication in a transmission electron microscope. *Nano Lett* 7:1329–1337.
15. Li J, Banhart F (2004) The engineering of hot carbon nanotubes with a focused electron beam. *Nano Lett* 4:1143–1146.
16. Rodríguez-Manzo JA, et al. (2007) In situ nucleation of carbon nanotubes by the injection of carbon atoms into metal particles. *Nat Nanotechnol* 2:307–311.
17. Sun L, et al. (2006) Carbon nanotubes as high-pressure cylinders and nanoextruders. *Science* 312:1199–1202.
18. Kamalakaran R, et al. (2000) Synthesis of thick and crystalline nanotube arrays by spray pyrolysis. *Appl Phys Lett* 77:3385.
19. Elías AL, et al. (2005) Production and characterization of single-crystal FeCo nanowires inside carbon nanotubes. *Nano Lett* 5:467–472.
20. Banhart F, Füller T, Redlich P, Ajayan P (1997) The formation, annealing and self-compression of carbon onions under electron irradiation. *Chem Phys Lett* 269:349–355.

21. Golberg D, et al. (2006) In-situ electrical probing and bias-mediated manipulation of dielectric nanotubes in a transmission electron microscope. *Appl Phys Lett* 88:123101.
22. Wang M, Wang J, Chen Q, Peng L (2005) Fabrication and electrical and mechanical properties of carbon nanotube interconnections. *Adv Funct Mater* 15:1825–1831.
23. Kresse G, Hafner J (1993) Ab initio molecular dynamics for liquid metals. *Phys Rev B* 47:558–561.
24. Kresse G, Hafner J (1994) Ab initio molecular-dynamics simulation of the liquid-metal-amorphous-semiconductor transition in germanium. *Phys Rev B* 49:14251–14269.
25. Kresse G, Furthmüller J (1996) Efficiency of ab-initio total energy calculations for metals and semiconductors using a plane-wave basis set. *Comput Mater Sci* 6:15–50.
26. Kresse G, Furthmüller J (1996) Efficient iterative schemes for ab initio total-energy calculations using a plane-wave basis set. *Phys Rev B* 54:11169–11186.
27. Kresse G, Joubert D (1999) From ultrasoft pseudopotentials to the projector augmented-wave method. *Phys Rev B* 59:1758–1775.
28. Blöchl P (1994) Projector augmented-wave method. *Phys Rev B* 50:17953–17979.
29. Perdew J, Burke K, Ernzerhof M (1996) Generalized gradient approximation made simple. *Phys Rev Lett* 77:3865–3868.
30. Balderschi B, Baroni S, Resta R (1988) Band offsets in lattice-matched heterojunctions: A model and first principles calculations for GaAs/AlAs. *Phys Rev Lett* 61:734–737.
31. Meunier V, Roland C, Bernholc J, Buongiorno-Nardelli M (2002) Electronic and field emission properties of boron nitride/carbon nanotube superlattices. *Appl Phys Lett* 81:46.
32. Jiang D, Sumpter BG, Dai S (2006) Structure and bonding between an aryl group and metal surfaces. *J Am Chem Soc* 128:6030–6031.
33. Xue Y, Ratner M (2004) End group effect on electrical transport through individual molecules: A microscopic study. *Phys Rev B* 69:085403.
34. Dujardin E, Ebbesen TW, Hiura H, Tanigaki K (1994) Capillarity and wetting of carbon nanotubes. *Science* 265:1850–1852.
35. Skriver H, Rosengaard N (1992) Surface energy and work function of elemental metals. *Phys Rev B* 46:7157–7168.
36. Jiang D, Carter E (2003) Carbon dissolution and diffusion in ferrite and austenite from first principles. *Phys Rev B* 67:214103.
37. Banhart F, Redlich P, Ajayan P (1998) The migration of metal atoms through carbon onions. *Chem Phys Lett* 292:554–560.
38. Banhart F, Charlier J, Ajayan P (2000) Dynamic behavior of nickel atoms in graphitic networks. *Phys Rev Lett* 84:686–689.